EFFECTS OF SUBMERGED WEIR WITH AN OPENING ON BED DEFORMATION AND FLOW STRUCTURE UNDER LIVE-BED CONDITIONS

HIROTAKA UNE
Graduate School of Science and Technology, Kumamoto University, Japan, 181d9201@st.kumamoto-u.ac.jp

TERUNORI OHMOTO
Civil and Environmental Engineering, Kumamoto University , Japan, ohmoto@kumamoto-u.ac.jp

KAZUKI KURANAGA
Graduate School of Science and Technology, Kumamoto University, Japan, 190d8307@st.kumamoto-u.ac.jp

ABSTRACT

Scouring or depositing downstream of submerged weirs with an opening is a sediment phenomenon resulting from the interaction of the three-dimensional turbulent flow field around the structure and the moveable sand bed. This paper presents the experimental study on the downstream bed topography due to weir with square shape of an opening, paying attention to the effects of non-dimensional relative tractive force on local scouring around the structure and three-dimensional flow patterns. The experiments were conducted under the live bed condition for an equilibrium scour hole. The experimental results show that local scouring holes have a similarity in shape and their maximum scouring holes around the structure depend on relative tractive force. Three-dimensional flow pattern with cellular secondary currents show the strong correlation with the scouring hole.

Keywords: *submerged weir with an opening, river bed morphology, local Scouring, live-bed conditions three-dimensional turbulent flow, cellular secondary currents*

1. INTRODUCTION

River transverse structures such as dams and weirs have been benefiting people for many years in terms of water use and flood control. On the other hand, they interrupt the hydraulic and ecological continuity of rivers and bring about various problems. For example, a fixed weir, which is a transverse river structure, interrupt sediment transport within a river then the interruption of the sediment transportation, cause the following issues: i) sediment accumulates on the upstream side of the weir, and the original water service function is lowered. ii) Deposit of sediment on the upstream side of the weir increases the water level on the upstream side during flooding, resulting in increased flood risks. iii) On the downstream side of the fixed weir, physical and biological environments disappear and tend to suppress natural disturbance. iv) The river bed in the downstream side is eroded because the supply of sediment from upstream of the fixed weir is interrupted by the weir (Miwa 1994). From this background, fixed dams are sometimes replaced with movable dams due to the consolidation of dams. However enormous expenses are required for dredging and construction of sediments in advance.

There are many weirs in Japan, and it is not practical to replace all of them with movable weirs. The authors (Ohmoto et al. 2016 and 2017, Une et al. 2018) have proposed that an existing fixed weir be created with an opening that opens when water flows out. The following effects can be expected by providing an opening and approaching a natural river. 1) The dredging cost can be reduced by flowing sediment accumulated in the upstream area of the weir for many years at the time of flooding. Maintenance is easy. 3) Reduction of sediment accumulation on the upstream side leads to a decrease in water level at the time of flooding, and improvement of flood control safety can be expected. 4) Due to sediment transport from upstream, improvement of environmental functions can be expected on the downstream side due to recovery of physical and biological environment and increase of natural disturbance. On the other hand, it is necessary to study the effect of weirs with openings on riverbed variation and flow. However, few studies have examined the effects of weirs with openings on riverbed changes in previous studies.

Zhang et al. (2012) conducted a series of experiments using a flume bedded with various materials having different grain sizes and specific gravities and various weirs with an opening and investigated scour

characteristics of the channel bed upstream of a submerged weir and local flows over the weir. Sumida et al. (2015) performed experiments using a flume having a relatively large width-to-height ratio and investigated the effects of weir opening geometry and size on the channel bed processes upstream of the weir resulting from scouring. However, there are few studies that have looked at the influence of a weir with an opening on channel bed processes downstream of the weir, and have dealt with the effects of a weir with an opening on sediment scour and deposition characteristics and flow regime of the channel bed downstream.

Depending on the conditions of sediment transport upstream of the weir, local scours are classified as clear water scour and live bed scour. In clear water scour, local scour is gradually formed without sediment supply from the upstream, whereas in live bed scour, the local scouring process becomes complex due to supplying the sediment from the upstream of the weir. Melville(1997) reviewed past studies on bridge piers and abutments and presented an empirical formula for calculating the maximum scour depth. It has been reported that the maximum scouring depth of piers and abutments is maximum when the ratio of the approach average flow velocity to the upstream of the structure and the critical approach average flow velocity of particles is 1, and becomes smaller under the live bed scour. Dawei Guan et al.(2014), (2015) discussed scour patterns of a river bed immediately downstream of a weir and flow patterns and turbulence characteristics of such a river channel and pointed out that secondary currents occur immediately downstream of the weir, showing clearly discernible three-dimensional flow structures, even if the weir is uniform in shape in the cross-stream direction. In live bed condition, an empirical formula for scour depth was proposed through a dimensionless analysis that the scouring mechanism around the weir depends on the strength of the approaching flow and the form of the flow over the weir.

The authors and others (Ohmoto et al. 2016 and 2017, Une et al. 2018) examined the effect of a weir with an opening on the riverbed variation downstream of a static equilibrium bed, and the three-dimensionality and turbulence structure of the flow over a sandbar developed downstream of the weir. In this study, the opening of the weir was made rectangular, and the three-dimensional structure of the riverbed morphology and flow in the static and dynamic equilibrium beds above and below the dive weir were examined.

2. EXPERIMENTAL SETUP

Table1. Experimental conditions

Case	Discharge Q(l/s)	Flow depth h(cm)	Mean velocity Um(cm/s)	Friction velocity u_*(cm/s)	Dimensionless tractive force τ_*	u_*/u_{*c}	τ_*/τ_{*c}	Froude number Fr
1	3.3	5.5	15.4	1.07	0.009	0.52	0.26	0.21
2	4.4	5.5	20.5	1.43	0.016	0.7	0.47	0.27
3	5.5	5.5	24.6	1.72	0.024	0.84	0.71	0.34
4	6.4	5.6	29.1	2.03	0.033	0.99	0.97	0.39
5	8.5	6.3	34.7	2.38	0.046	1.16	1.35	0.44
6	10.5	6.7	40.2	2.74	0.06	1.33	1.76	0.5
7	15.4	7.5	52.8	3.54	0.101	1.72	2.97	0.61

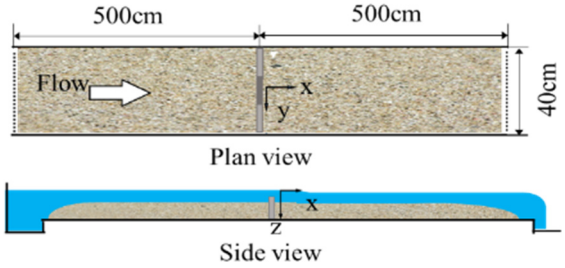

Figure 1. Experimental channel

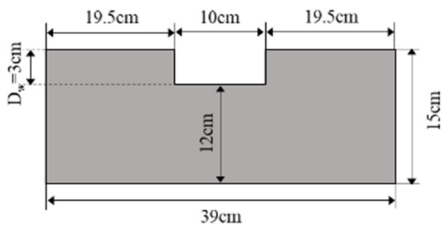

Figure 2. Weir model

The experiments were conducted with a 10-m-long, 40-cm-wide, 20-cm-deep variable-slope circulating acrylic flume. As shown in Figure 1, the weir shown in Figure 2 was installed 5m downstream from the upstream end. The sediment which median diameter d_{50}=0.77mm and relative submerged particle density 1.65 was laid on the upstream and downstream of the weir. The sediment is uniform with standard deviation 1.29. The experiment was conducted continuously from clear water condition to live bed condition. Table 1 shows the experiment conditions. In this study, the channel slope I=1/300 was set to facilitate the movement of sediment. The experiment was performed by changing the flow rate Q=3.3 to 15.43 l/s. However, the water level was adjusted by the weir at the downstream end. In the table, Um and h are the mean cross-sectional velocity and water depth at 3 m upstream of the weir, u_* is the friction velocity, u_{*c} is the critical friction velocity, τ_* is the dimensionless

tractive force, and *Fr* is the Froude number. The critical friction velocity u_{*c} was calculated from the median grain size of the bed material, and the friction velocity was calculated by the logarithmic law. The equivalent sand roughness k_s was calculated at $2d_{50}$. Movement of the bed material upstream of the weir is a condition that is static in Cases 1-4 and dynamic in Cases 5-7.

The origin of the coordinate system is located at the center of the bottom of the flume where the opening is located. The right-hand coordinate system has an *x*-axis in the flow direction, a *y*-axis in the cross-stream direction, and a *z*-axis in the vertical downward direction. Their flow velocity components are represented by u, v and w; their time average components by *U*, *V* and *W*; and their variable components by *u*', *v*' and *w*'. Water level and bed height were measured with a point gauge and an ultrasonic water level sensor, respectively. For the investigation of flow mechanisms, point measurement and multi-point simultaneous measurement of water surface profile and flow velocity were made in Case 2-4 shown in Table 1. Surface flow measurement was made by the PIV (particle image velocimetry) method using a video camera system capable of multi-point simultaneous measurement of flow velocity, and the point measurement of flow velocity was made with one component and two-component electromagnetic current meters. In the flow velocity measurement by the PIV method, water surface profile was video-recorded from directly above the flume for a period of 20 seconds, and nylon particles having a particle size of 100 μm and a specific gravity of 1.02 were used as a tracer. Visualization image data were recorded on a computer's hard disk in the form of 59.94 fp (frames per second) 1920×1080-pixel black-and-white image data and were processed by the PIV method. The 100Hz output signals from the electromagnetic current meters were processed with an analog-to-digital converter, and data for a total of 4,096 data sets were statistically processed for each measuring point.

3. EXPERIMENTAL RESULTS

3.1 Bed deformations

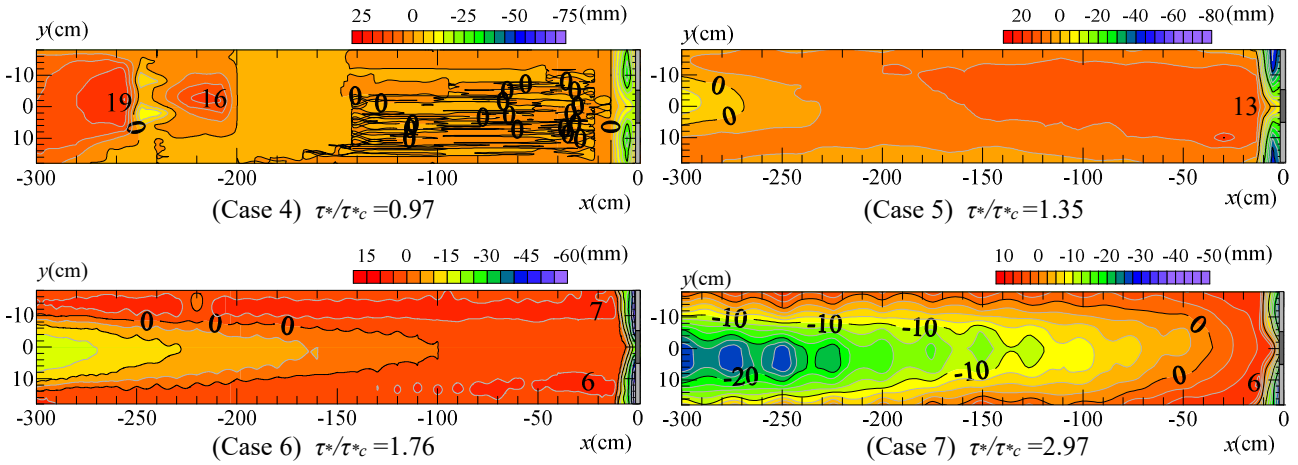

Figure 3. Bed deformation of the upstream of the weir

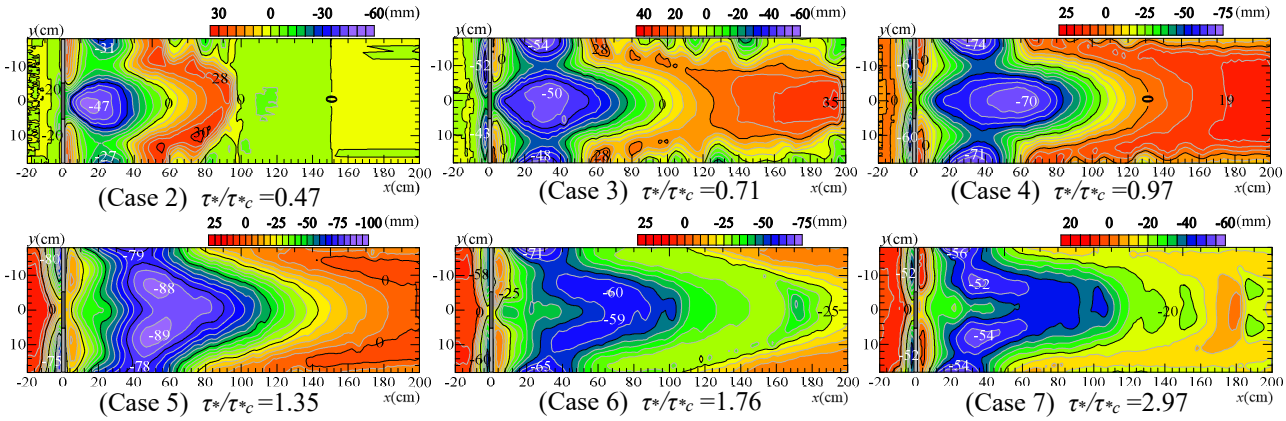

Figure 4. Bed deformation of the upstream and downstream of the weir

Figure 3 shows the contours of the bed height at the upstream of the weir in Cases 4 to 7, where the movement of sediment on the upstream side was confirmed. The contour figures show the amounts of changes (in millimeters) from the initial flat bed figures. In Case 4, the sediment upstream of the weir began to move, and a sand bar formed 200 cm upstream of the weir. When the tractive force was further increased, it was confirmed that the sand bar propagated immediately upstream of the weir and that sediment was transported downstream through the opening. It can be seen that the maximum sediment thickness of the sand bar upstream of the weir

occurs at y= 0 cm upstream of the opening in Case 4 and Case 5 and occurs at y= -11 cm and y= 11 cm in Case 6 and Case 7, respectively.

Figure 4 shows the contours of the bed height immediately upstream and downstream of the weir. In addition, the numerical value of the contour shows the amount of change from the initial flat bed in millimeter. Case 2 to Case 4 are under clear water condition, and Case 5 to Case 8 are under live bed condition. It can be seen that the local scouring upstream of the weir occurs in the range of y= -8cm to -10cm near the opening in Case2, but in the range of y= -18cm to -5cm and y= 5cm to 18cm in Cases 3 to 7. The scour depth increases with increasing tractive force in a static equilibrium bed. In this local scour, it is considered that a vortex with a transverse axis was formed by the flow that collided with the weir, and the vortex lifted up the sediment and transported it downstream of the weir through the opening.

It can be seen that the maximum scour downstream of the weir in the static equilibrium riverbed occurs downstream of the opening. On the other hand, it can be seen that the maximum scour downstream of the opening occurs in the range of y = -10 ~ 10cm in the transverse direction. In Case 2, Case 3 and Case 4, the maximum water depth at the center of the channel downstream of the weir is 107.8 mm, 108.0 mm and 117.6 mm, respectively. The maximum scour downstream of the opening has a spatial scale of about twice the maximum water depth downstream of the weir. The maximum scouring downstream of the opening is x = 58 cm at τ_*/τ_{*c}= 0.47, x=96 cm at τ_*/τ_{*c}= 0.71 and x=130cm at τ_*/τ_{*c}= 0.97. and it can be seen that it expands in the downstream direction as the tractive force increases. This is considered that the sediment downstream was swept because the flow velocity passing through the opening increased with the increase of the tractive force.

At τ_*/τ_{*c}= 1.35 ~ 2.97, which is under live-bed condition, it can be seen that the planar spread of scour downstream of the opening is larger than that of the static equilibrium bed. The transverse scale of the maximal scour downstream of the opening is y=-14 to 14 cm at τ_*/τ_{*c}=1.35, y=-12 to 12 cm at τ_*/τ_{*c}=1.76 and y=−12 to 13 cm at τ_*/τ_{*c}=1.76. In Case 5, Case 6 and Case 7, the maximum water depth at the center of the channel downstream of the weir is 143 mm, 127 mm and 122 mm, respectively, and has a spatial scale of about twice the maximum water depth downstream of the weir.The maximum scouring depth is the largest at τ_*/τ_{*c}= 1.35. The maximum scouring depth tends to decrease compared to τ_*/τ_{*c}= 1.35 when τ_*/τ_{*c}= 1.76 and τ_*/τ_{*c}= 2.97.

On the other hand, the sediment downstream of the weir occurs downstream of the scour hole, and the spatial distribution of the sediment spreads downstream as the tractive force increases. In addition, in this experimental result, the maximum deposition thickness becomes maximum at τ_*/τ_{*c}= 0.71 at 35 mm and shows a decreasing tendency as the tractive force increases. At τ_*/τ_{*c}= 1.35 ~ 2.97, which is the dynamic equilibrium bed condition, there is no significant deposition downstream of the weir.

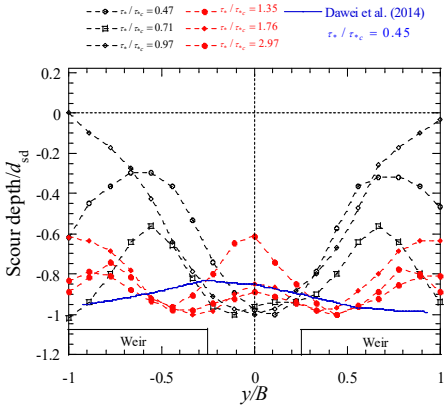

Figure 5 Transverse profile of the bed height of the downstream of the opening

Figure 5 shows the cross-section of the bed at the maximum scouring depth downstream of the opening. The scouring depth and transverse direction y were dimensionless with the maximum scouring depth d_{sd} and channel width B, respectively. It can be seen that in both under static equilibrium condition and dynamic equilibrium condition, the bed is relatively high near the left and right walls compared to the downstream of the opening. This suggests that a downward flow occurs in the center of the canal and an upward flow occurs near the side walls.The cross section of the bed profile at the maximum scouring depth at the downstream of the non-opening weir is indicated by the blue line. According to Dawei et al. (2014), downstream of the non-opening weir under the clear water condition, the upward flow occurs in the center of the channel and downward flow occurs near the left and right walls. As the results maximum scouring occurs near the left and right walls. Comparing to the results of opening and non-opening weir, it is presumed that the flow structure is significantly different.

Figures 6 and 7 show the longitudinal and cross-sectional bed profile of scouring upstream of the weir, respectively. The scouring depth and longitudinal distance x in Figure 6 were nondimensionalized by the

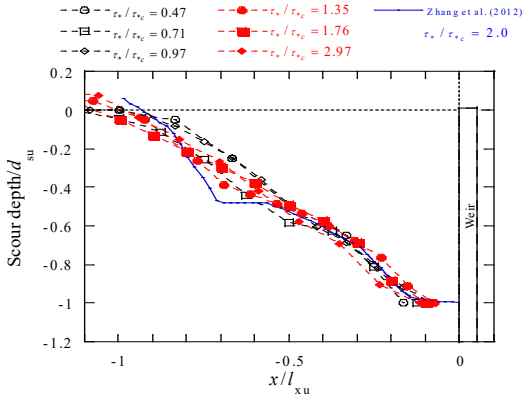

Figure 6. Longitudinal profile of scouring upstream of the weir

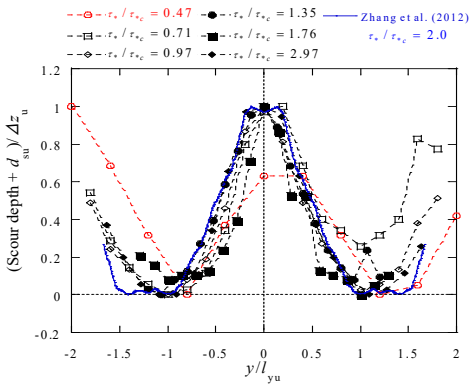

Figure 7. Transverse profile of scouring upstream of the weir

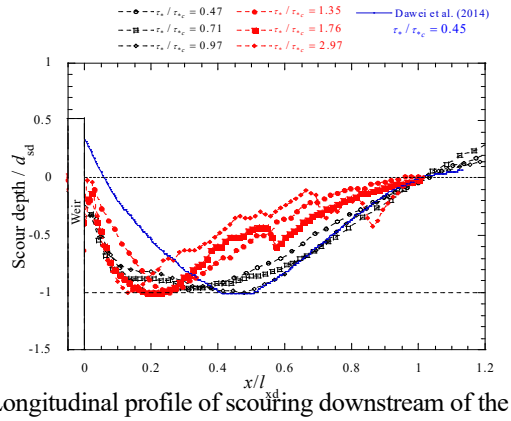

Figure 8. Longitudinal profile of scouring downstream of the weir

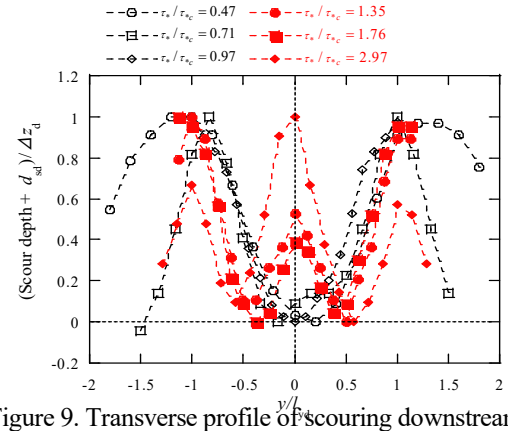

Figure 9. Transverse profile of scouring downstream of the weir

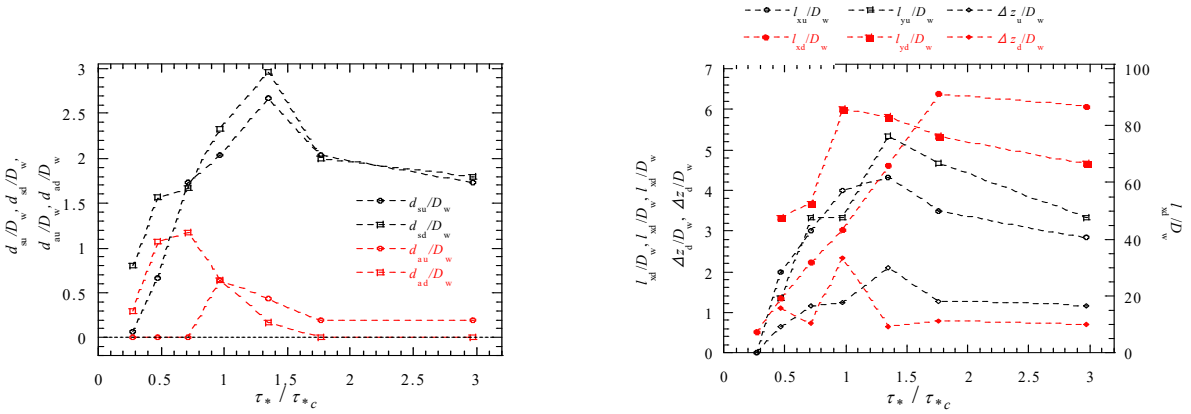

Figure 10. the characteristics of bed deformation and tractive force.

maximum scouring depth d_{su} and scouring length l_{xu} upstream of the weir, respectively. The scour depth in Figure 7, is normalized by the maximum scour depth d_{su} and the difference Δz_u between the ridge and the trough of the bed height, and the transverse direction distance y is normalized by the width l_{yu} between the troughs of the bed profile. In the figure, the experimental results by Zhang et al. (2012) are plotted in blue for reference. The longitudinal bed profile of scouring upstream of the weir is similar in all cases, it can be seen that the scour depth rises almost linearly from downstream to upstream. A comparison the experimental results of Zhang et al., Shows that although there is a slight difference in the range of x/l_{xu}=0.65 to 0.75, they almost agree with each other. Except for τ_*/τ_{*c}= 0.47, the cross-sectional shape of scouring upstream of the weir was found to be W-shaped and similar the experimental results by Zhang et al. (2012).

Figures 8 and 9 show the longitudinal and transverse bed profile of scouring downstream of the weir, respectively. The scouring depth and longitudinal distance x in Figure 8 were nondimensionalized by the maximum scouring depth d_{sd} and scouring length l_{xd} downstream of the weir, respectively. The scour depth in In Figure 9, scour depth is normalized by the maximum scour depth d_{sd} and the difference Δz_d between the ridge and the trough of the bed height, and the transverse direction distance y is normalized by the width l_{yd} between the troughs of the bed profile. The longitudinal profile of scouring downstream of the weir is similar in the range of τ_*/τ_{*c}= 0.47 to 0.97, which is in the static equilibrium bed. On the other hand, the longitudinal profile of scouring downstream of the weir is similar in the range of τ_*/τ_{*c}= 1.35 to 2.97, which is in the live bed. In downstream from the maximum scour, the bed gradient in the dynamic equilibrium bed is more gradual than in the static equilibrium bed. However, it can be seen that the distribution in the range of x/ l_{xd} = 0.45 to 1.0 the bed height with the non-opening is almost the same as our experimental result of the static

equilibrium bed. The cross-sectional shape of the bed at the position where the maximum scouring depth occurs downstream of the opening is similar to the M-shape in the range of τ_*/τ_{*c}= 0.47 ~ 0.97 which is a static equilibrium bed. In the cross-sectional shape of τ_*/τ_{*c}= 1.35 ~ 2.97, which is a dynamic equilibrium bed, the bed becomes higher at the center of the channel and shows a similar tendency in a W shape.

Figures 10 show the changes in the characteristics of maximum scour depth, sediment thickness and bed shape with respect to the tractive force. Each parameter is nondimensionalized by the weir height D_w. The change of the maximum scouring depth upstream and downstream with respect to the tractive force increases almost linearly in the range of tractive force τ_*/τ_{*c}= 0.26 to 1.35, and the magnitude of the maximum scouring depth upstream and downstream, Corresponds to about 3 times and 2.7 times the weir height at the largest τ_*/τ_{*c}= 1.35, respectively. On the other hand, the maximum scouring depth at tractive force τ_*/τ_{*c}= 1.76 and 2.97 was smaller than that at tractive force τ_*/τ_{*c}= 1.35. The maximum scouring depth upstream and downstream of the weir at τ_* / τ_{*c} = 2.97 decreases to 65% and 60%, respectively, for the tractive force τ_*/τ_{*c}= 1.35. This tendency has been reported in local scouring of piers (Melville 1997) and non-opening weirs (Dawei et al. 2015), and it is probable that scour holes were backfilled by sediment supply from upstream.

The maximum sediment thickness d_{au} upstream of the weir is the largest at τ_*/τ_{*c}= 0.97 and decreases with increasing tractive force. The maximum sediment thickness dad downstream of the weir tends to increase as the tractive force increases in the range of tractive force τ_*/τ_{*c}= 0.26 to 0.71, but the tractive force τ_*/τ_{*c}= It can be seen that there is a decreasing tendency in the range of 0.97 to 2.97.The downstream scour length l_{xu} upstream of the weir, the transverse scour length l_{yu}, and the difference Δz_u between the peak and the valley of the bed height are the tractive forces τ_* / τ_{*c} in the range of 0.47 to 1.35. It can be seen that the scouring length l_{xu} and scouring length l_{yu} tend to decrease and the difference in bed height Δz_u is constant at tractive forces τ_*/τ_{*c}= 1.76 and 2.97.

It can be seen that the scouring length l_{xd} in the downstream direction increases linearly with increasing tractive force in the range of tractive force τ_*/τ_{*c}= 0.26 to 1.76. When the tractive force τ_* / τ_{*c} is larger than 1.76, the scouring length l_{xd} in the downstream direction becomes almost constant. The downstream scour length l_{xd}, transverse scour length l_{yd}, and the difference Δz_d between the peak and valley of the bed height downstream of the weir tend to increase in the range of tractive force τ_*/τ_{*c}= 0.26 to 0.97. It can be seen that the tractive force is declining and almost constant in the range of tractive force τ_*/τ_{*c}= 0.26 to 1.76.

3.1 Local flow on the downstream of the weir opening

Figures 11 to 13 show the plane contours of the main flow velocity U, the transverse component V of the secondary flow, and the vertical component W in Case 3 and Case 6, respectively, measured 1 cm above the top of the weir. The main velocity U, the transverse component V and the vertical component W of the secondary flow were nondimensionalized by the average cross-sectional velocity of each case. It can be seen that the main flow velocity U in the upper layer of the weir top in Case 3 and Case 6 is relatively fast under the influence of the overflow at x= 0-15cm immediately downstream of the weir. Also, within the range of y = -5cm to 5cm downstream of the opening, the main flow velocity U is relatively fast at -5cm <y <5cm, which falls downstream of the weir opening, and the low-speed region is -18cm <y <-5cm and 5cm. <y <18cm.

In Case 3, the high-speed region where U/U_m> 1 is larger than the cross-sectional average flow velocity, gradually narrows down in the range of x=20 to 80 and is formed at y= -5cm-5cm. It can be seen that the high-speed region gradually expands downstream in the range of x= 80cm to 100cm further downstream. It is considered that the flow velocity was accelerated downstream of x= 60cm from the bed shape in Case 3 (Fig. 5), because the bed height increased as the distance from the weir increased. On the other hand, in Case6, in the range of x= 20-70cm, the high-speed region tends to gradually decrease in the downstream direction like Case3, but it is wider in the transverse direction than Case3 and is formed at y= -8cm-8cm.

The magnitude of the transverse component V and vertical component W of the secondary flow downstream of the weir was about 20% of the average cross-sectional velocity at the largest in both Case 3 and Case 6, and very large flows were confirmed. The transverse component V of the secondary flow can be confirmed in Case 3 in the range of x= 0 to 60 cm downstream of the weir, with the convergent flow at the center of the channel and the divergent flows at y= -14 cm and y= 13 cm. On the other hand, downstream of x= 60cm, a divergent flow is shown at the center of the channel. In Case 6, the flow is weak but diverges at the center of the channel, and convergent regions are observed at y= -6cm and y= 5cm.

The vertical component W of the secondary flow in Case 3 shows a downward flow downstream of the weir and downstream of the opening. The spatial distribution of the downward flow downstream of the opening decreases and sharply contracts with the downward flow, and upward flows are observed on the left and right sides. The spatial distribution of the vertical component W of the secondary flow in Case 6 shows that

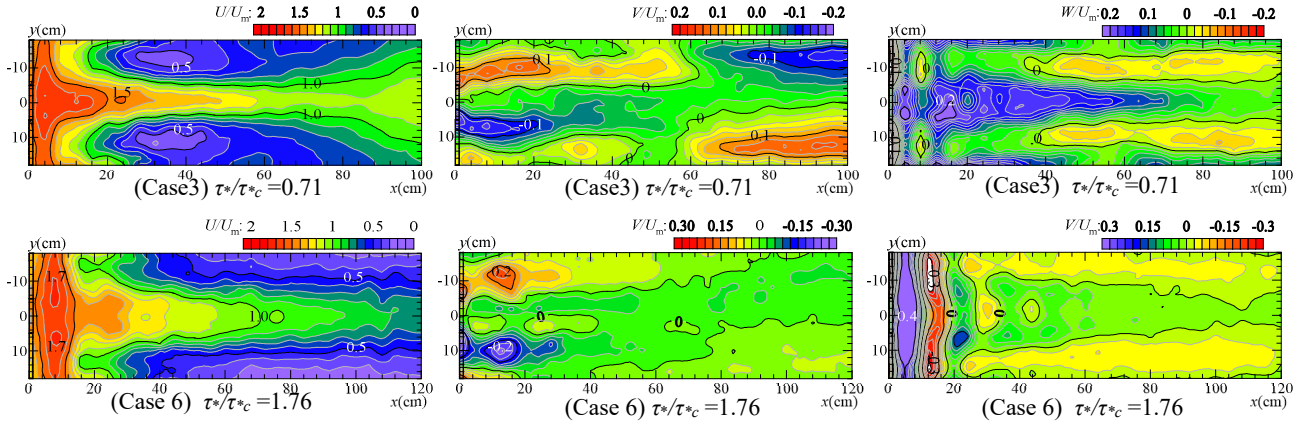

Figure 11. Main flow velocity contours Figure12. Secondary flow velocity *V* contours Figure 13. Secondary flow velocity *W* contours

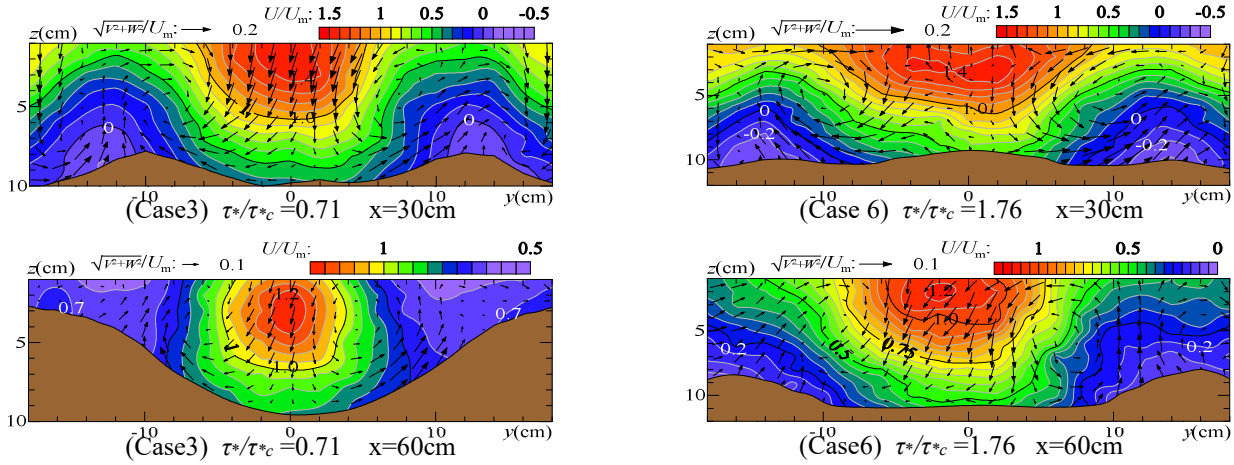

Figure 14. Main flow velocity contours and secondary flow vectors

immediately below the weir, the ascending flow and the descending flow alternately occur in the section where the water surface fluctuation is large *x*= 40cm. Downstream, it shows the same tendency as Case 3.

Figure 14 shows the contour map of the main flow velocity *U* in the vertical plane, which is nondimensionalized by the cross-sectional average flow velocity at *x*= 30 cm and 60 cm downstream of the weir in Case 3 and Case 6, respectively. In the figure, the combined vector of the transverse component *V* and the vertical component *W* of the secondary flow is shown, and the size of the secondary flow vector is nondimensionalized by the cross-sectional average velocity U_m.

The downstream of the weir, secondary flow cells were confirmed in both Case 3 and Case 6. In each case, there is a correlation between the location of the upward flow and the downward flow of the secondary flow and the bed shape, and it can be seen that the downward flow and the upward flow occur at the valley and the peak of the bed, respectively. The downward flow diverging at the bottom at *x*= 30cm in Case 3 falls in the range of *y*= -5cm to 5cm, which hits the valley of the bed downstream of the opening. It can be seen that it occurs at 9 cm and *y*= 9 cm to 12 cm. On the other hand, the downward flow at *x*= 30 cm in Case 6 is *y*= -9 cm to -6 cm and *y*= 5 cm to 10 cm, and the upward flow occurs at *y*= -14 cm to -11 cm and *y*= 12 cm to 15 cm. It can be seen that the secondary flow cell is generated slightly to the side walls.

In Case3 and Case6, the size of the secondary flow is smaller at *x*= 60cm than at *x*= 30cm. In addition, the downward flow at *x*= 60cm is only in the range of *y*= -5cm-5cm, which falls downstream of the opening, and the upward flow occurs near the side walls, and the bed is relatively rising. Compared with the experimental results of non-opening weirs9), it can be seen that the secondary flow cell is formed in the opposite direction by the opening, and the bed is relatively high.

The main flow velocity *U* is relatively high in the section of the weir opening *y*= -5cm to 5cm at *x*= 30cm in both Case3 and Case6, and the maximum flow velocity shows a slight downward tendency. The main velocities in the sections *y*= -18cm to -5cm and *y*= 5cm to 18cm over the top of the weir fall in the relatively low speed region, and the spatial variation of the main velocities in the vertical direction is large due to the effect of the weir. Although a strong shear layer is formed, the change in the vertical direction becomes smaller at *x*= 60 cm, and the high-speed region is observed only in the section at *y*= -5 cm to 5 cm downstream of the opening. The spatial distribution of the main flow velocity U has a relationship with the spatial

distribution of the secondary flow, and the contour line of the main flow velocity U is convex downward in the descending basin and upward convex in the ascending basin. It is inferred that advection was caused by.

The spatial distribution of the main flow velocity U at x= 60cm indicates that the flow velocity at the y= -18cm to -5cm and y= 5cm to 18cm, which falls behind the weir, decreases with the flow near the water surface. This indicates that the low velocity fluid mass near the bottom was advected to near the water surface due to the strong upward flow on the left and right walls. It is considered that the high-velocity region near the water surface converges to the center of the river channel by the secondary flow, and the low-speed fluid mass near the bottom surface is advected on the left and right walls.

4. CONCLUSIONS

In this study, the opening of the weir was made into a rectangular shape, and the bed form and flow structure of the static and dynamic equilibrium beds upstream and downstream of the dive weir were examined. The main results obtained are as follows.

1) Scouring downstream of the weir with an opening concentrates immediately downstream of the opening, and the surface spread of the scouring increases as the tractive force increases.
2) The longitudinal and cross-sectional shapes of scour upstream of the weir were similar to the tractive force. Furthermore, the longitudinal and cross-sectional shapes of scour downstream of the weir are similar in M-shape in static equilibrium bed and similar in W-shape in dynamic equilibrium bed.
3) The change in the maximum scouring depth upstream and downstream with respect to the tractive force increases almost linearly in the range of tractive force τ_*/τ_{*c}= 0.26 to 1.35. It can be seen that the maximum scour depth at τ_*/τ_{*c}=1.76 and τ_*/τ_{*c}=2.97 is smaller than that at tractive force τ_*/τ_{*c}= 1.35.
4) The slope angle on the upstream side and the slope angle on the downstream side in the central part of the channel downstream of the weir decrease exponentially with increasing tractive force.
5) In the upstream area of the weir, a strong downward flow appeared near the opening of the weir. In the downstream area of the weir, correlation with the bed shape was observed. In the peak of the bed, an upward flow and a downward flow converging in the valley were observed.

REFERENCES

Hajime M. (1994). Diversion Dam Problems on Alluvial Streams. *Journal of the Agricultural Engineering Society*. Volume 62 Issue 5 Pages 421-426,a1.

Terunori O., Tatsuhiro Y., Hirotaka U. (2016). EFFECTS OF WEIR WITH AN OPENING ON RIVER BED AND FLOW STRUCTURE. *Journal of Japan Society of Civil Engineers, Ser. B1 (Hydraulic Engineering).* Volume 72 Issue 4 Pages I_811-I_816.

Terunori O., Hirotaka U. (2017). EFFECTS OF UPWARD WEIR WITH AN OPENING ON RIVER BED AND FLOW STRUCTURE. *Journal of Japan Society of Civil Engineers, Ser. B1 (Hydraulic Engineering)*. Volume 73 Issue 4 Pages I_703-I_708.

Hirotaka U., Terunori OHMOTO (2018). EFFECTS OF OBLIQUE WEIR WITH AN OPENING ON RIVER BED AND FLOW STRUCTURE. *Journal of Japan Society of Civil Engineers, Ser. B1 (Hydraulic Engineering)*. Volume 74 Issue 5 Pages I_829-I_834.

Zhang H., Muto, Y., Nakagawa, H and Nakanishi, S. (2012): Weir removal and its influence on hydro-morphological features of upstream channel, Journal of applied mechanics, Vol.15, No2, pp.591-599.

Sumida H.,Muto Y.,Tamura T.(2015).CHANNEL TO DEVELOPMENT ON UPSTREAM DUE TO CHANGE OF PARTIALLY REMOVED WEIR, *Journal of Japan Society of Civil Engineers,Ser.B1 (Hydraulic Engineering)*, Vol.71,No.4.I925-I930

Bruce W. Melville (1997). Pier and Abutment Scour: Integrated Approach, J. *Hydraulic Engineering,, ASCE*, Vol.123, No.2,,pp.125-136.

Dawei G. , Bruce W. Melville, Heide Friedrich (2014).Flow Patterns and Turbulence Structures in a Scour Hole Downstream of a Submerged Weir. *J.Hydraulic Engineering*. Vol.140,No.1,pp.68-76.

Dawei G. , Bruce W. Melville, Heide Friedrich (2015). Live-Bed Scour at Submerged Weirs. *J.Hydraulic Engineering*. Vol.141,No.2,Paper No.04014071.

Tsutomu K. and Mikio K. (1972). Bed Forms and Resistance to Flow in Erodible-Bed Channels (1)-Hydraulic Relations for Flow over Sand Waves- . *Hokkaido University Collection of Scholarly and Academic Papers. HUSCAP*. 67, 1-23.